PAPER

Check for updates

Synthesis through 3D printing: formation of 3D coordination polymers†

Oded Halevi,[abc] Jingwei Chen,[bc] Gurunathan Thangavel,[b] Samuel Alexander Morris,[b] Tal Ben Uliel,[d] Yaakov Raphael Tischler,[d] Pooi See Lee [ID] *[bc] and Shlomo Magdassi [ID] *[ac]

Coordination polymers (CPs) and coordination network solids such as metal–organic frameworks (MOFs) have gained increasing interest during recent years due to their unique properties and potential applications. Preparing 3D printed structures using CP would provide many advantages towards utilization in fields such as catalysis and sensing. So far, functional 3D structures were printed mostly by dispersing pre-synthesized particles of CPs and MOFs within a polymerizable carrier. This resulted in a CP active material dispersed within a 3D polymeric object, which may obstruct or impede the intrinsic properties of the CP. Here, we present a new concept for obtaining 3D free-standing objects solely composed of CP material, starting from coordination metal complexes as the monomeric building blocks, and utilizing the 3D printer itself as a tool to *in situ* synthesize a coordination polymer during printing, and to shape it into a 3D object, simultaneously. To demonstrate this, a 3D-shaped nickel tetra-acrylamide monomeric complex composed solely of the CP without a binder was successfully prepared using our direct print-and-form approach. We expect that this work will open new directions and unlimited potential in additive manufacturing and utilization of CPs.

Introduction

Coordination polymers (CPs) belong to a highly interesting family of materials, which are 1D, 2D and 3D macro molecules, comprised of metal ions that are linked by ligands, usually organic molecules (Fig. 1a). CPs have become popular in the past twenty years, since the rise of the sub-group of porous CPs, known as metal–organic frameworks (MOFs),[1] among other groups of promising porous functional materials.[2,3] The interest in CPs started in the early 1950's,[4] and this group of extended inorganic–organic assemblies includes many additional porous and non-porous compounds, which have interesting chemical properties and applications in a wide variety of fields. Most of the reports focus on the molecular design, synthetic chemistry and their applications in heterogeneous catalysis, gas storage and molecular separation. For example, Soo Seo *et al.* reported

the synthesis of a porous coordination polymer for the catalysis of an enantioselective transesterification reaction;[5] Du *et al.* synthesized a silver coordination polymer for highly selective sensing of Cd^{2+};[6] and Wang *et al.* explored coordination polymer particles with antibacterial and anticancer activity.[7]

With the advent of additive manufacturing that effectuates the emergence and quick adoption of three-dimensional (3D) printing, bottom-up fabrication of functional 3D-objects have been realized rapidly. For example, functional reaction-ware, shape-customized adsorbing structures, 3D catalysts and batteries are a few examples that can be achieved through 3D printing with the layer-by-layer deposition of materials, according to a predesigned computer 3D model.[8] 3D printing enables formation of customized and complex structures with minimum material waste and high precision.[9] Initially, the most commonly printed materials were organic polymers. More recently, the potential of 3D-printing has pored over to the discovery of unique materials properties and the development of new fabrication processes inclusive of metals,[10] ceramics and hydrogels.[11,12] The properties of the resulting 3D objects are dependent on the printing technology; for example, light initiated printing, such as digital light processing printers (DLP) (Fig. S1†), is based on localized UV-polymerization of liquid formulations, layer over layer, to form solid 3D-structures. Typical inks for this technology are composed of photo-initiators and monomers, and in some cases dispersed or dissolved materials. Two interesting approaches were recently

[a] Casali Center for Applied Chemistry, Institute of Chemistry, The Hebrew University of Jerusalem, Jerusalem, 91904, Israel. E-mail: magdassi@mail.huji.ac.il

[b] School of Materials Science and Engineering, Nanyang Technological University, 639798, Singapore. E-mail: pslee@ntu.edu.sg

[c] Singapore-HUJ Alliance for Research and Enterprise (SHARE), Nanomaterials for Energy and Energy-Water Nexus (NEW), Campus for Research Excellence and Technological Enterprise (CREATE), 138602, Singapore

[d] Department of Chemistry, Bar-Ilan University, Ramat-Gan, 5290002, Israel

† Electronic supplementary information (ESI) available. CCDC 1979541. For ESI and crystallographic data in CIF or other electronic format see DOI: 10.1039/d0ra01887b

reported: Greer *et al.*, used two-photon lithography printing of monomers with nickel-containing photoresist, resulting in a structure containing more than 90 wt% Ni-containing architecture after pyrolysis of the organic materials.[13] Hanrath *et al.*, modified oxozirconium nanoclusters with methacrylic acid and printed hierarchical and highly porous architectures.[14]

In the past two years, there have been several reports of functional 3D-printed structures that contained coordination polymers. Thakkar *et al.* reported the 3D-printing of MOF, embedded in an organic–inorganic binder for removal of CO_2 from air,[15] as well as the 3D-printing of ZIF-7 embedded within organic monoliths for ethane/ethylene separation processes.[16] Our group reported the 3D-printing of Cu-BTC MOF for the adsorption of organic dyes from solutions,[17] and Lyu *et al.* reported a 3D-printed cobalt-based MOF embedded within an organic binder for energy storage applications.[18] More examples on 3D-printed MOFs were explored by Lawson *et al.* and Sultan *et al.*[19,20] Recently, our group, in collaboration with Amo-Ochoa and Zamora, also published the 3D-printing of a Cu^{2+} coordination polymer for the colorimetric sensing of humidity and water.[21]

In these prior works, the coordination polymers were synthesized prior to the printing, mostly in the form of particles, which were later dispersed within matrix forming materials, since the CP particles could not form a stand-alone 3D object without binders. Therefore, so far, the resulting printed objects are composed of CPs embedded within organic or inorganic binders. A direct print-and-form route to prepare free

standing coordination polymer objects with 3D architecture has not been realized. Herein we present an approach, in which we form 3D objects composed solely of a coordination polymer, while the printing process causes both the synthesis of the coordination polymer, and the formation of a free standing 3D object.

Results and discussion

Our approach differs from the traditional pathway to the synthesis of CPs in which metal ions were reacted with bridging ligands, which have more than one metal-binding site (Fig. 1a).[22] Another possibility, although challenging and not common, is to bind non-bridging ligands to the metal ions to form inorganic complexes, and then connect these ligands to one another (Fig. 1b). Such metal-containing-monomers (MCMs)[23–27] have both polymerizable functional groups and electron donating groups, such as acrylamide and acrylic acid (Fig. 1c). In these attempts, the polymerization was initiated mostly by heating.

By proper selection of ligands that can polymerize upon exposure to ultra-violet (UV) light, we hypothesize that rationally designed and formulated MCMs can be utilized as 3D inks that can form free-standing objects without any additional binders or monomers, by light initiated printing processes. Therefore, the printing can be utilized both as a tool to synthesize the coordination polymer, and to directly obtain 3D structures composed predominantly of the coordination polymer, that can be tailored according to the required application. To demonstrate this approach, we have synthesized MCM with a Ni^{2+} metal center and acrylamide ligands, and formulated it as a photo-polymerizable ink, without any additional monomers. The ink composition was 3D-printed by a DLP printer, resulting in a stand-alone complex structure of an amorphous coordination polymer.

In this work, nickel(II) was selected as the metal for the MCM, since it demonstrates rich chemistry and is being utilized for various applications, mostly for catalysis. For example: Cui *et al.* synthesized a Ni^{2+} CP and demonstrated its photocatalytic activity in degradation of water pollutants;[28] Ghorbani-Choghamarani *et al.* immobilized Ni^{2+} complexes on boehmite nanoparticles for the heterogeneous catalysis of sulfides oxidation to sulfoxides, and oxidative coupling of thiols into disulfides;[29] and Malgas *et al.* synthesized dendritic Ni^{2+} catalysts for ethylene oligomerization.[30] Therefore, we have first synthesized the photo-polymerizable Ni containing monomer, followed by its conversion into a coordination polymer by 3D-printing process.

For a proof of concept for the new approach, we synthesized a MCM based on nickel and acrylamide ligands, $[Ni(AAm)_4(H_2O)_2](NO_3)_2$ (**Ni complex**).[31] The MCM was obtained as a wet powder, which was then recrystallized into a single crystal from ethanol, and its structure was determined for the first time (Fig. 2a, b and Table S1†). As shown, the complex has interesting features: the octahedral complex comprises four acrylamide ligands bonded to the Ni^{2+} center *via* the carbonyl oxygen, and two water molecules in axial positions. The
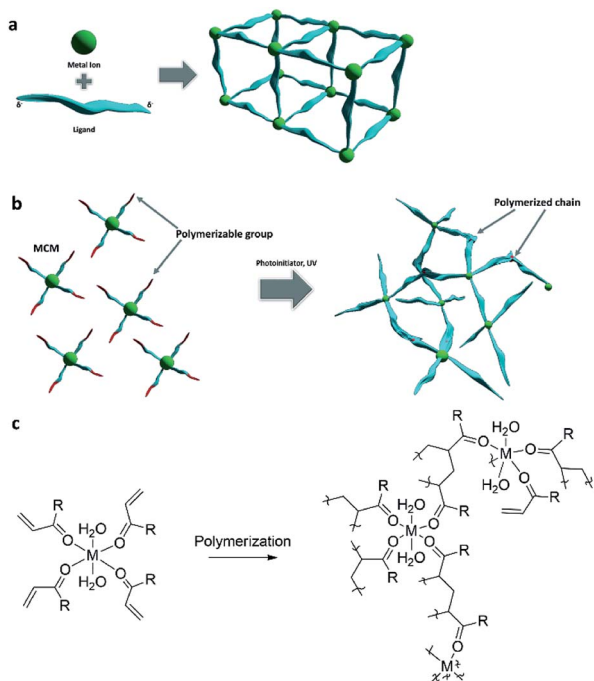
Fig. 1 (a) CP formation by reacting metal ions with bridging ligands. (b) CP formation by polymerization of MCMs. (c) The hypothesized polymerization reaction of the MCM with polymerizable acryl ligands. "R" represents any functional group or organic residue attached to the acryl group.
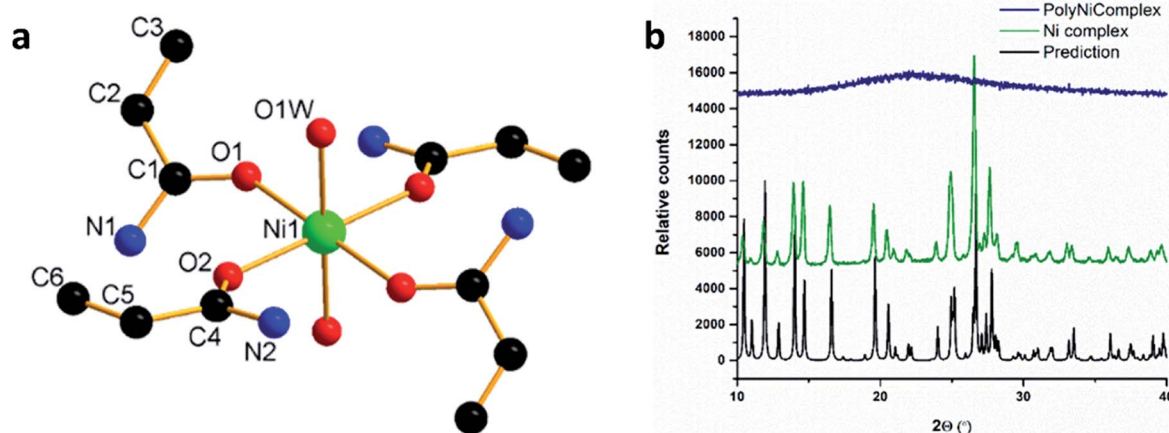
Fig. 2 (a) Crystal structure of the $[Ni(AAm)_4(H_2O)_2]^{2+}$ complex, hydrogen atoms and the nitrate anions were removed for clarity. (b) PXRD prediction, based on the single crystal structure, and the measured diffractograms for **Ni complex** and the **polyNiComplex**.

presence of the coordinative water molecules has high significance for future utilizations of the MCM polymerization product, as it may provide two available positions on the polymeric Ni^{2+} ion, and its potential binding to other electron-donating molecules. Powder X-ray diffraction measurement (PXRD) (Fig. 2b) confirmed that the crystal structure of the wet powder was identical to the single crystal. Further investigation of the structure by Fourier Transform Infra-Red (FTIR)
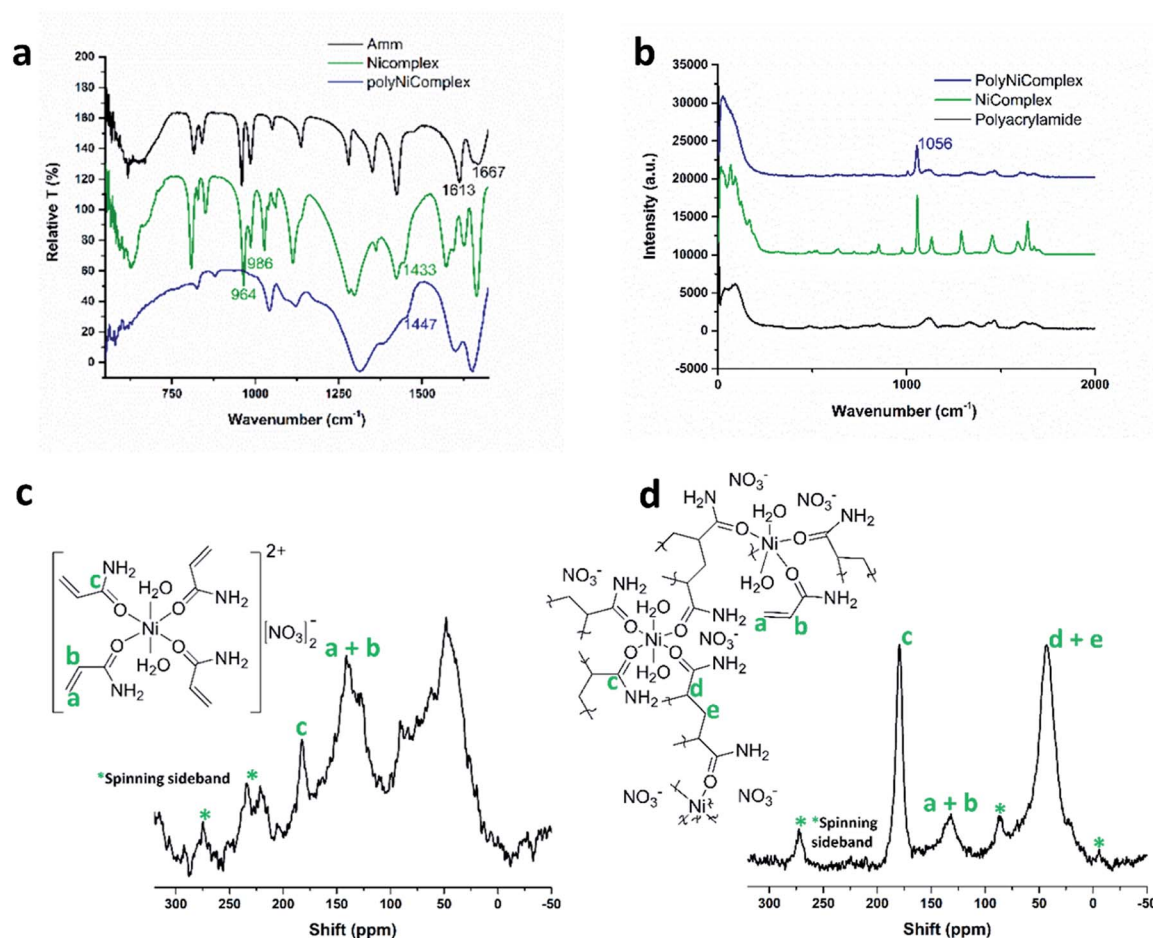

Fig. 3 (a) FTIR spectra of the free acrylamide, **Ni complex**, and **polyNiComplex**. (b) Raman spectra of the **polyNiComplex**, **Ni complex**, and polyacrylamide. (c) Solid-state ^{13}C NMR of **Ni complex**. (d) Solid-state ^{13}C NMR of **polyNiComplex**.

spectroscopy (Fig. 3a) shows a spectrum similar to one of the free acrylamide. Following complexation, an expected redshift and splitting of the bands at 1670 cm^{-1} and 1613 cm^{-1} is observed; this corresponds well with the previously reported FTIR spectra of other acrylamide metal complexes.[23] The characteristic peak of the non-coordinative nitrate ion, around 1400 cm^{-1}, can be identified as a shoulder at 1443 cm^{-1} in the **Ni complex** spectrum.

3D objects of the coordination polymer (**polyNiComplex**) were printed successfully by the DLP printer (Fig. 4a), while using the MCM as the single monomer in the solution, without any additional monomers. Since the synthesized MCM has four acrylamide ligands, it could function as a built-in cross-linker. The MCM was dissolved in absolute ethanol at a weight ratio of 1 : 2 respectively, and a photo-initiator, diphenyl (2,4,6-trimethylbenzoyl)phosphine oxide (TPO) was added at a low concentration (2 %wt). It should be noted that the printed object remained covered by the ethanol solution throughout the whole printing process, thus avoiding problems arising from the hygroscopic nature of the CP. Once the printing was complete, the 3D-CP object was exposed to UV light for additional five minutes, in order to react any unpolymerized monomers on the surface, followed by a thorough washing with ethanol and drying under vacuum.

An interesting feature of the printed CP, which was revealed by scanning electron microscopy (SEM), is its macroporous structure (Fig. 4b). As shown, the whole 3D object is composed of connected spherical particles, which as will be proven in the following section, are composed of the coordination polymer. This is of high importance in view of future applications in which surface area is essential, such as in diagnostics, catalysis and separation processes. The measured surface area of the grinded sample revealed that the printed material has a surface area of 53.32 ± 23.00 m^2 g^{-1}. The measured isotherm (Fig. S2†), combined with the calculated pores size of 35.90 ± 24.80 Å, suggests a mesoporous structure. Currently, further investigation of the porosity and its tuning, as well as the influence of the macro structure of the 3D-printed objects on the total accessible surface area of the CP is underway, and will be the focus of a future report.

A major challenge following the 3D-printing process, was to identify whether the Ni–O bond of the nickel-acrylamide remained intact during the radical polymerization reaction; and whether the printed object was indeed a coordination polymer. PXRD of the printed polymer was performed (Fig. 2b) and it was found that it is non-crystalline. FTIR measurements (Fig. 3a) indicated that the polymerization reaction indeed occurred, as the peaks for C=CH and C=CH$_2$ at 986 cm^{-1} and 964 cm^{-1} disappeared in the polymer spectrum.[23] However, the Ni–O bond could not be identified, as it was predicted to be around 400–500 cm^{-1}.[32–34] As in the **Ni complex** salt, the nitrate ion was also present in the polymerized product, as indicated by the shoulder at 1447 cm^{-1}. Furthermore, Raman spectroscopy (Fig. 3b) revealed the presence of the nitrate ions in the printed polymer, with their Raman shift appearing at 1056 cm^{-1}.[35] Nuclear magnetic resonance (NMR) was considered in order to extract more information on the nickel environment. [61]Ni NMR was not practical due to the paramagnetism of Ni^{2+}, however solid ^{13}C NMR revealed more information (Fig. 3c and d). For the monomer NMR, the peak at 56.28–34.93 ppm, indicates saturated CH$_2$, as well as CH carbons, revealing that during the drying process, that is following the synthesis and washing steps, partial polymerization took place. Therefore, the monomer was used without drying, immediately after the synthesis and washings. For the polymer, the decrease of the ^{13}C NMR peak at 140–126 ppm revealed that the C=C bond decreased and a C–C bond was formed instead.[36,37] So far, the organic part of the hypothesized CP was well characterized, however there was no direct indication regarding the Ni^{2+} species and its immediate chemical environment in the polymer.

Focusing on the nickel, there were three questions to be addressed: first, was the distribution of the nickel in the polymer uniform, or was there a phase-separation between the Ni^{2+} and the polyacrylamide? Second, has there been any loss of nickel ions during the printing or the washings? Third, was the nickel still bonded to the carbonyl oxygen of the acrylamide? The first question was addressed by energy-dispersive X-ray spectroscopy measurements (EDX), which showed a uniform distribution of the nickel throughout the whole printed structure (Fig. S3†); thus it was concluded that no phase-separation occurred. For the second question, inductively coupled plasma optical emission spectrometry (ICP-OES) measurements were conducted. The results in Table 1 show that the amount of nickel in the object after the washing step remained the same as that at the beginning of the process, within the error range.

To verify the existence of Ni–O bonds, we compared the binding energies of the Ni^{2+} before and after polymerization, by X-ray photoelectron spectroscopy (XPS) (Fig. S4†). The binding energies of MCM Ni 2p$_{1/2}$ and Ni 2p$_{3/2}$ are located at 873.8 eV and 856.3 eV respectively, indicative of the presence of Ni^{2+} (typical Ni–O=C binding energy) in the MCM (Table 1).[38] After the printing/polymerization process, there were no shifts of the binding energies of Ni 2p$_{1/2}$ and Ni 2p$_{3/2}$ in **polyNiComplex**, indicating no change in chemical environment of Ni^{2+} before and after polymerization. To further investigate the Ni–O bond
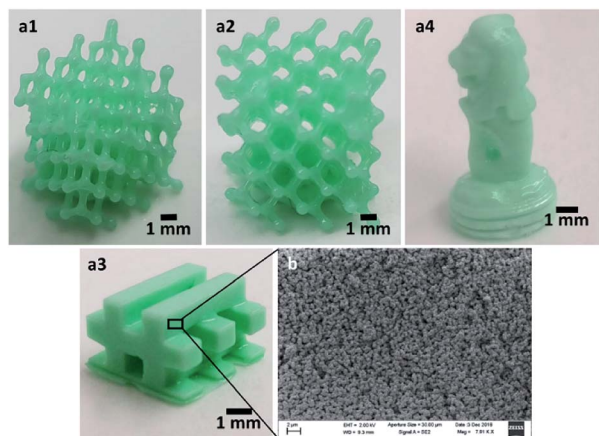

Fig. 4 (a) Various 3D-printed structures of **polyNiComplex**. (b) SEM of the printed **polyNiComplex** cross-section.

Table 1 Nickel weight percentage and binding energies in the **Ni complex** and **polyNiComplex**, as measured by ICP-OES and XPS, respectively

Sample	Ni wt% by ICP-OES	Ni $2p_{3/2}$ [eV]	Ni $2p_{1/2}$ [eV]	O 1s [eV]
Ni complex	6.4 ± 1.6	856.3	873.8	533.1, 532.5
PolyNiComplex	7.4 ± 0.3	856.3	873.8	532.4

after polymerization, the oxygen bonding energies before and after polymerization were analysed by XPS as well (Fig. S5,† Table 1). Before polymerization, two peaks, located at binding energies of 533.1 and 532.5 eV were deconvoluted. The minor peak located at 533.1 eV is assigned to the water molecules present in the complex.[39] The other major peak at 532.5 eV is assigned to the $Ni(OCNH_2)$ bond.[40] After polymerization, the O1s spectra is deconvoluted to one peak located at 532.4 eV, which is also ascribed to the $Ni(OCNH_2)$ bond. The slight downshift of the binding energy of this peak after polymerization was tentatively attributed to the polymerization induced stretching of $H_2N–C\!\!=\!\!O–Ni$. These results, combined with ^{13}C NMR and Raman spectroscopy, indicated that the Ni^{2+} ions remained bonded to the carbonyl oxygen, forming a positively charged coordination polymer stabilized with nitrate ions. Thus, it could be concluded that a coordination polymer was indeed successfully synthesized by 3D-printing.

Conclusions

In summary, this paper presents a synthetic print-and-form strategy through the utilization of light-based 3D-printing as a synthesis tool for coordination polymers. This work has two interesting aspects; first, synthesis-wise, for the first time a transition-metal complex was used as a monomer for synthesis of pure CP by using a 3D printer as a synthesis tool. The second important aspect of this work is the ability to form complex structures of stand-alone CPs, thus opening the pathways for their utilization for various applications that require complex architectures, such as reactive flow reactors, separation columns, and reaction-ware with built-in catalysts. Although the current work focused on Ni-acrylamide complexes, we expect that the variety of metal ions and polymerizable ligands will enable the synthesis through printing of many other amorphous or crystalline CPs, with tailored functionality that takes advantage of free standing complex 3D objects.

Experimental

Synthesis of $[Ni(AAm)_4(H_2O)_2](NO_3)_2$ (Ni complex)

$Ni(NO_3)_2 \cdot 6H_2O$ (Sigma) (2.5 g) and acrylamide (AAm) (Sigma)(3.0 g) were mixed and grinded together with a mortar and pestle for several minutes. As the reaction progressed, water was released and the reaction mixture turned from dark to light green. Following this, the product was washed three times with chloroform (VWR) and three times with diethyl ether (Sigma). Single crystals were obtained by recrystallization from ethanol. Solid-state ^{13}C NMR $[Ni(AAm)_4(H_2O)_2](NO_3)_2$: (600 MHz, δ)

56.28–34.93 ($–CH_2$, $–CH$), 145.93–126.61 ($–CH\!\!=\!\!CH_2$), 186.60–178.51 ($–C\!\!=\!\!O$), *: spinning sideband.

3D-printing of polyNiComplex

Ni complex was dissolved in absolute ethanol (VWR), in a 1 : 2 weight ratio, respectively. The photoinitiator, Irgacure TPO (BASF) (2 wt%), was added to the solution. The 3D-structures were printed with the DLP 3D-printer (Asiga Pico 2, 405 nm). The printing parameters are shown in Table S2.† Following the printing, the structures were exposed to UV-light for 5 minutes, washed with absolute ethanol three times and placed under vacuum at room temperature overnight.

Solid-state ^{13}C NMR of poly$[Ni(acrylamide)_4(H_2O)_2](NO_3)_2$

(600 MHz, δ) 56.88–32.67 ($–CH_2$, $–CH$), 140.75–126.09 ($–CH\!\!=\!\!CH_2$, $–CH_2–CH_2–$), 188.32–173.94 ($–C\!\!=\!\!O$), *: spinning sideband.

Characterization methods

The characterization of the **Ni complex** and **polyNiComplex** was done with Powder X-ray Diffraction (Shimadzu, XRD-6000), Single-crystal X-ray Diffraction (Bruker, SMART APEX II) CCDC 1979541, Fourier Transform Infra-Red (PerkinElmer, Frontier), Home built micro-Raman Spectroscopy setup (Olympus, BXFM combined with Ondax, THz-Raman filter coupled to Princeton Instruments, SP-2500i), Surface area measurements (Micromeritics, ASAP-2020) – the surface area was calculated according to the Brunauer–Emmett–Teller (BET) model. Prior to the surface area measurement, the 3D-printed structures were gently grinded with a mortar and pestle, and degassed for 12 h at 50 °C. The following tools were also used for characterization: Inductively Coupled Plasma Optical Emission Spectrometry (PerkinElmer, Optima 8300), Scanning Electron Microscopy (Carl Zeiss, SUPRA 55), Energy-Dispersive X-ray Spectroscopy (JEOL, FESEM 7600F), X-ray Photoelectron Spectroscopy (Kratos Analytical, Axis Ultra), and solid-state ^{13}C NMR (Bruker, Avance III HD 600 MHz,14.1 T, wide-bore MAS solid-state NMR spectrometer).

Conflicts of interest

There are no conflicts to declare.

Acknowledgements

Notes and references

1 H. Furukawa, K. E. Cordova, M. O'Keeffe and O. M. Yaghi, *Science*, 2013, **341**, 974.

2 S. Yuan, X. Li, J. Zhu, G. Zhang, P. Van Puyvelde and B. Van der Bruggen, *Chem. Soc. Rev.*, 2019, **48**, 2665–2681.

3 Y. Li, L. Li and J. H. Yu, *Chem*, 2017, **3**, 928–949.

4 K. Biradha, A. Ramana and J. J. Vittal, *Cryst. Growth Des.*, 2009, **9**, 2969–2970.

5 J. S. Seo, D. Whang, H. Lee, S. I. Jun, J. Oh, Y. J. Jeon and K. Kim, *Nature*, 2000, **404**, 982–986.

6 P. Y. Du, W. Gu, S. Gao and X. Liu, *Inorg. Chem. Commun.*, 2015, **60**, 47–50.

7 K. B. Wang, X. Y. Ma, D. L. Shao, Z. R. Geng, Z. Y. Zhang and Z. L. Wang, *Cryst. Growth Des.*, 2012, **12**, 3786–3791.

8 J. Horvath, *Mastering 3D Printing*, Apress, 2014.

9 T. D. Ngo, A. Kashani, G. Imbalzano, K. T. Q. Nguyen and D. Hui, *Composites, Part B*, 2018, **143**, 172–196.

10 J. H. Martin, B. D. Yahata, J. M. Hundley, J. A. Mayer, T. A. Schaedler and T. M. Pollock, *Nature*, 2017, **549**, 365–369.

11 C. Minas, D. Carnelli, E. Tervoort and A. R. Studart, *Adv. Mater.*, 2016, **28**, 9993–9999.

12 H. J. Li, C. Tan and L. Li, *Mater. Des.*, 2018, **159**, 20–38.

13 A. Vyatskikh, S. Delalande, A. Kudo, X. Zhang, C. M. Portela and J. R. Greer, *Nat. Commun.*, 2018, **9**, 593.

14 J.-Y. Huang, H. Xu, E. Peretz, D.-Y. Wu, C. K. Ober and T. Hanrath, *Chem. Mater.*, 2019, 10017–10022.

15 H. Thakkar, S. Eastman, Q. Al-Naddaf, A. A. Rownaghi and F. Rezaei, *ACS Appl. Mater. Interfaces*, 2017, **9**, 35908–35916.

16 H. Thakkar, Q. Al-Naddaf, N. Legion, M. Hovis, A. Krishnamurthy, A. A. Rownaghi and F. Rezaei, *ACS Sustainable Chem. Eng.*, 2018, **6**, 15228–15237.

17 O. Halevi, J. M. R. Tan, P. S. Lee and S. Magdassi, *Adv. Sustainable Syst.*, 2018, **2**, 1700150.

18 Z. Y. Lyu, G. J. H. Lim, R. Guo, Z. K. Kou, T. T. Wang, C. Guan, J. Ding, W. Chen and J. Wang, *Adv. Funct. Mater.*, 2019, **29**, 1806658.

19 S. Lawson, Q. Al-Naddaf, A. Krishnamurthy, M. S. Amour, C. Griffin, A. A. Rownaghi, J. C. Knox and F. Rezaei, *ACS Appl. Mater. Interfaces*, 2018, **10**, 19076–19086.

20 S. Sultan, H. N. Abdelhamid, X. D. Zou and A. P. Mathew, *Adv. Funct. Mater.*, 2019, **29**, 1805372.

21 N. Maldonado, V. G. Vegas, O. Halevi, J. I. Martinez, P. S. Lee, S. Magdassi, M. T. Wharmby, A. E. Platero-Prats, C. Moreno, F. Zamora and P. Amo-Ochoa, *Adv. Funct. Mater.*, 2019, **29**, 1808424.

22 S. Benmansour and C. J. Gomez-Garcia, *Polymers*, 2016, **8**, 89.

23 K. B. Girma, V. Lorenz, S. Blaurock and F. T. Edelmann, *Z. Anorg. Allg. Chem.*, 2005, **631**, 2763–2769.

24 K. B. Girma, V. Lorenz, S. Blaurock and F. T. Edelmann, *Z. Anorg. Allg. Chem.*, 2005, **631**, 1843–1848.

25 I. E. Uflyand, I. A. Ilchenko, A. G. Starikov, V. N. Sheinker and A. D. Pomogailo, *Bull. Acad. Sci. USSR, Div. Chem. Sci.*, 1990, **39**, 388–391.

26 V. S. Savostyanov, V. I. Ponomarev, A. D. Pomogailo, B. S. Selenova, I. N. Ivleva, A. G. Starikov and L. O. Atovmyan, *Bull. Acad. Sci. USSR, Div. Chem. Sci.*, 1990, **39**, 674–679.

27 V. S. Savostyanov, A. D. Pomogailo, B. S. Selenova, D. A. Kritskaya and A. N. Ponomarev, *Bull. Acad. Sci. USSR, Div. Chem. Sci.*, 1990, **39**, 680–684.

28 J. W. Cui, S. X. Hou, Y. H. Li and G. H. Cui, *Dalton Trans.*, 2017, **46**, 16911–16924.

29 A. Ghorbani-Choghamarani, B. Tahmasbi, F. Arghand and S. Faryadi, *RSC Adv.*, 2015, **5**, 92174–92183.

30 R. Malgas, S. F. Mapolie, S. O. Ojwach, G. S. Smith and J. Darkwa, *Catal. Commun.*, 2008, **9**, 1612–1617.

31 V. S. Savostyanov, D. A. Kritskaya, A. N. Ponomarev and A. D. Pomogailo, *J. Polym. Sci., Part A: Polym. Chem.*, 1994, **32**, 1201–1212.

32 J. Fujita, K. Nakamoto and A. E. Martell, *J. Chem. Phys.*, 1962, **36**, 324–331.

33 C. Djordjevic, *Spectrochim. Acta*, 1965, **21**, 1018–1020.

34 V. S. Savostyanov, V. N. Vasilets, O. V. Ermakov, E. A. Sokolov, A. D. Pomogailo, D. A. Kritskaya and A. N. Ponomarev, *Bulletin of the Russian Academy of Sciences-Division of Chemical Science*, 1992, **41**, 1615–1620.

35 S. Ramaswamy, M. Umadevi, R. K. Rajaram and V. Ramakrishnan, *J. Raman Spectrosc.*, 2003, **34**, 806–812.

36 G. Garnweitner, B. Smarsly, R. Assink, W. Ruland, E. Bond and C. J. Brinker, *J. Am. Chem. Soc.*, 2003, **125**, 5626–5627.

37 Y. Sugahara, S. Satokawa, K. Kuroda and C. Kato, *Clays Clay Miner.*, 1990, **38**, 137–143.

38 M. O. de Souza, F. M. T. Mendes, R. F. de Souza and J. H. Z. dos Santos, *Microporous Mesoporous Mater.*, 2004, **69**, 217–221.

39 E. Desimoni and B. Brunetti, *Chemosensors*, 2015, **3**, 70–117.

40 T. Yoshida, K. Yamasaki and S. Sawada, *Bull. Chem. Soc. Jpn.*, 1978, **51**, 1561–1562.